

Phase diagram of α -helical and β -sheet forming peptides

Stefan Auer¹ and Dimo Kashchiev²

¹Centre for Molecular Nanoscience, University of Leeds, Leeds LS2 9JT, United Kingdom

²Institute of Physical Chemistry, Bulgarian Academy of Sciences,

Ul. Acad. G. Bonchev 11, Sofia 1113, Bulgaria

(Dated: October 25, 2018)

The intrinsic property of proteins to form structural motifs such as α -helices and β -sheets leads to a complex phase behaviour in which proteins can assemble into various types of aggregates including crystals, liquid-like phases of unfolded or natively folded proteins, and amyloid fibrils. Here we use a coarse-grained protein model that enables us to perform Monte Carlo simulations for determining the phase diagram of natively folded α -helical and unfolded β -sheet forming peptides. The simulations reveal the existence of various metastable peptide phases. The liquid-like phases are metastable with respect to the fibrillar phases, and there is a hierarchy of metastability.

In a diagram of protein solution (e.g., refs[1–4]), the solubility line specifies the conditions under which a protein crystal neither grows nor dissolves and corresponds to the gas-crystal coexistence line in a diagram of atomic system. Similarly, the gas-liquid coexistence line for an atomic system corresponds to the liquid-liquid separation line for a protein solution (the latter is the line of coexistence of two separate liquid phases, a protein-rich and a solvent-rich ones). The phase behavior described in refs[1, 2, 4] involves native proteins, with little or no difference in the protein conformation in the different phases. However, depending on solvent conditions and physical variables such as temperature, the proteins may also adopt non-native conformations, resulting in the formation of various aggregates. Indeed, a wide range of different proteins unrelated in their amino acid sequence have been shown to form amyloid fibrils which share a common characteristic cross- β structure where peptides form β -sheets oriented parallel to the fibril axis[5, 6]. Despite the importance of the effect of protein conformational changes on the protein phase diagram, we are aware of only one experimental diagram[3] involving this effect. It is for Human β B1-crystallin and describes the coexistence lines between a solution and fibrillar aggregates and between these aggregates and a liquid-like phase. On the other hand, attempts have also been made[7, 8] to numerically construct phase diagrams of peptides by determining the ground state structure of the condensed peptide phases. The resulting diagrams however do not account for the existence of metastable phases that are crucial to the understanding of generic aspects of the protein phase behavior.

The present study makes use of a novel theoretical framework[9] in which proteins are described as flexible tubes. In the model used here and described in detail elsewhere[10] the protein backbone is represented by a C_α chain with finite thickness. The directional hydrogen bonding is sequence-independent and can be accounted for by an analysis of the geometrical properties of hydrogen-bond forming C_α atoms in protein structures listed in the Protein Data Bank. The hydrogen-bond energy is denoted by ϵ . The hydrophobic effect between C_α atoms is captured by a pairwise attractive square-well po-

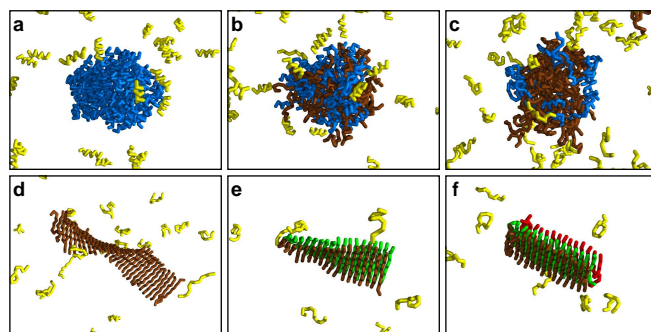


FIG. 1: Gallery of peptide aggregates. (a) α -oligomer at dimensionless temperature $\theta \equiv T/T_f = 0.9$, (b) and (c) γ -oligomer at $\theta = 1.0$ and 1.1 , respectively, (d) 1β -sheet at $\theta = 1.1$, (e) 2β -sheet at $\theta = 1.2$, and (f) 3β -sheet at $\theta = 1.2$. Peptides in the solution are shown in yellow, peptides within an aggregate that do not form interpeptide hydrogen bonds are shown in blue, and those that do so are shown in brown, green or red.

tential with energy ϵ_h . As in previous studies[10, 11], we use $\epsilon/\epsilon_h = 20$ in order to quantify the relative strength of the hydrogen and the hydrophobicity-mediated bondings. Steric constraints are implemented by a local bending stiffness with energy ϵ_s per C_α atom. In all our simulations the stiffness energy ϵ_s is set equal to 0.3ϵ . Peptides that are weakly hydrophobic, and hence have such a large ϵ/ϵ_h value, have been demonstrated[12] to assemble into the various types of aggregates considered here. We investigated the phase behavior of a simple prototype of biomolecular system consisting of 12-residue homopeptides in an implicit aqueous solution. The simulations showed that most of the peptides in the solution fold at least partially into a native α -helical structure at temperatures below the folding temperature $T_f = 0.20\epsilon/k$, and unfold at least partially into an extended random-coil structure above it. Our simulation model is thus pertinent to peptides with hydrogen-bond energy $\epsilon = (1.9 \text{ to } 2.5) \times 10^{-20}$ J, because these ϵ values correspond to $T_f = 276$ to 363 K, i.e. to peptide folding temperatures of biophysical relevance.

Our simulations showed that the peptides can self-assemble into different types of aggregates: α -oligomers -

disordered aggregates constituted solely of fully folded α -helical peptides (Fig. 1a), γ -oligomers - also disordered aggregates but consisting of fully folded, partially folded and unfolded peptides (Figs. 1b and 1c), and $i\beta$ -sheets - ordered aggregates with $i = 1, 2, 3, \dots$ layers of single β -sheet tapes (Figs. 1d-1f, respectively). Importantly, as seen in Figs. 1b and 1c, the fraction of folded/unfolded peptides in the γ -oligomers depends on temperature. We shall consider the above aggregates as representing distinct phases, because the relative contribution of the hydrophobicity-mediated and the hydrogen bondings that stabilize them is different (Fig. 2). While an α -oligomer is stabilized by the hydrophobicity-mediated bonding only, the γ -oligomer is additionally stabilized by the hydrogen bonding (by definition, a γ -oligomer is completely free of $i\beta$ -sheets). In contrast, the $i\beta$ -sheets are predominantly stabilized by the hydrogen bonding. On average (Fig. 2), for the number b of inter-peptide hydrogen bonds per peptide we have $b = 0$ for the α -oligomers, $b = 1$ or 3 for the γ -oligomers at dimensionless temperature $\theta \equiv T/T_f = 1.0$ or 1.1 , respectively, and $b = 18$ for all $i\beta$ -sheets. Also on average (Fig. 2), the number b_h of hydrophobicity-mediated bonds per peptide is 155 , 78 , 124 and 134 for the α -oligomer, 1β -sheet, 2β -sheet and 3β -sheet, respectively. For the γ -oligomer, $b_h = 132$ at $\theta = 1.0$ and 1.1 .

In order to determine the solubility lines for the α -oligomer, γ -oligomer and $i\beta$ -sheets with $i = 1, 2, 3$ we followed the approach used by Bai and Li[13]. We performed Monte Carlo simulations in the canonical ensemble using crankshaft, pivot, reptation, rotation and translation moves. The simulations were carried out by using a cubic box and periodic boundary conditions. For the α -oligomer solubility determination we prepared a cluster of a fixed number n of fully folded peptides and placed this n -sized cluster into a solution containing also a fixed number (100 or 200) of such peptides. Isothermally, we performed several simulation runs at different peptide concentrations and monitored whether the cluster grew or shrank. As in this case the cluster was an α -oligomer, we constrained the peptides in the system to remain fully folded by performing only rotation and translation moves during the simulation. This enabled us to calculate the α -oligomer solubility at temperatures at which the peptides would normally start to unfold. From the first simulation runs we identified two near peptide concentrations between which the α -oligomer would coexist with the solution. This provided a concentration range for additional runs which yielded more accurately the equilibrium concentration (or solubility) $C_{e,n}$ at which an n -sized α -oligomer neither grows nor shrinks. As cluster solubility is known to depend on cluster size, we studied the dependence of $C_{e,n}$ on n at a given θ by repeating our simulations for five α -oligomer sizes: $n = 100, 200, 300, 500$ and 700 . The results obtained are shown in Fig. 3a. The size dependence of $C_{e,n}$ can be described by the Ostwald formula (e.g., ref.[14])

$$\ln C_{e,n} = \ln C_e + a/\theta n^{1/3} \quad (1)$$

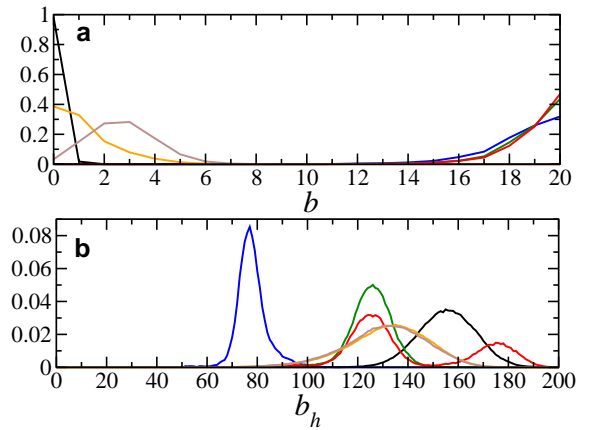


FIG. 2: Bonding in peptide aggregates. (a) Probability distribution function of the number b of hydrogen bonds per peptide in: α -oligomer (black line) at $\theta = 0.7$, γ -oligomer (orange line) at $\theta = 1.0$, γ -oligomer (brown line) at $\theta = 1.1$, 1β -sheet (blue line) at $\theta = 1.1$, 2β -sheet (green line) at $\theta = 1.2$, and 3β -sheet (red line) at $\theta = 1.2$. (b) Probability distribution function of the number b_h of hydrophobicity-mediated bonds per peptide in: α -oligomer (black line), γ -oligomers (orange and brown lines), 1β -sheet (blue line), 2β -sheet (green line), and 3β -sheet (red line) at the respective θ values noted above.

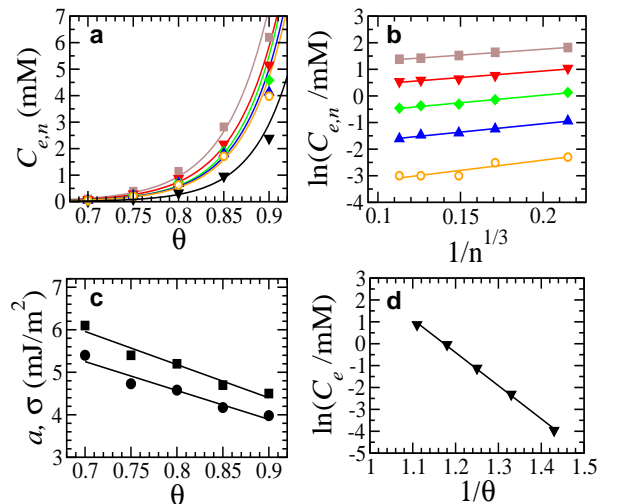


FIG. 3: α -oligomer results. (a) Temperature dependence of solubility: squares, open down triangles, diamonds, up triangles and circles - simulation data for cluster size $n = 100, 200, 300, 500$ and 700 , respectively; black triangles - derived data for $n = \infty$ from best-fit analysis; lines - best fit of equation 2. (b) Size dependence of solubility: squares, open down triangles, diamonds, up triangles and circles - simulation data at $\theta = 0.9, 0.85, 0.8, 0.75, 0.7$, respectively; lines - best fit of equation 1. (c) Dependence of parameter a (circles) and specific surface energy σ (squares) on θ ; the straight lines are drawn to guide the eye. (d) Solubility of bulk α -oligomeric phase: triangles - data from (a) for $n = \infty$; line - best fit of equation 2.

in which C_e is the equilibrium concentration (or solubility) of the infinitely large α -oligomer, and $a = 2c\sigma v^{2/3}/3kT_f$. Here σ is the specific surface energy of the α -oligomer/solution interface, v is the volume occupied by a peptide in α -oligomer, and for a spherical α -oligomer the shape factor $c = (36\pi)^{1/3}$. In $\ln C_{e,n}$ -vs- $1/n^{1/3}$ coordinates, a linear fit of equation 1 to our data (Fig. 3b) yielded values for $\ln C_e$ (from the intercept) at each temperature θ , and hence the solubility $C_e(\theta)$ of the infinitely large α -oligomer (the down triangles in Fig. 3a and in Fig. 4). Also, the slope of the fit provided the a value at each θ . The resulting $a(\theta)$ dependence (the circles in Fig. 3c) implies that the α -oligomer surface tension σ decreases with temperature as illustrated by the squares in Fig. 3c. These squares represent the σ values calculated from the above expression for a with the aid of $c = (36\pi)^{1/3}$ (spherical α -oligomers), $T_f = 300$ K (peptides with $\epsilon = 2.07 \times 10^{-20}$ J) and $v = 1.2$ nm³. The latter is the mid-range value of the peptide volume for θ between 0.7 and 0.9, and was obtained by dividing the volume of all peptides in the bulk of an α -oligomer by the number of these peptides. As seen in Fig. 3c, $\sigma = 4.5$ to 6.1 mJ/m² and is in the range of 0.1 to 30 mJ/m², values reported both theoretically and experimentally for the specific surface energy of protein crystals in aqueous solutions[2, 15, 16].

Fitting the integrated van't Hoff equation

$$C_e = C_r \exp(-\lambda/\theta) \quad (2)$$

to the $C_e(\theta)$ data in Fig. 3d enables determining the dimensionless latent heat $\lambda = L/kT_f$ of peptide aggregation into an infinitely large α -oligomer. Here C_r is a practically temperature-independent reference peptide concentration, and L is the latent heat of peptide aggregation into such an oligomer. The best-fit result is $C_r = 5.2 \times 10^7$ mM and $\lambda = 15.1 \pm 0.3$. With $T_f = 0.2\epsilon/k$ it thus follows that $L = \lambda kT_f$ has the value of 3ϵ . Hence, recalling that in our simulations $\epsilon = 20\epsilon_h$ and that on average $b_h = 155$, we find that the latent heat $L = 60\epsilon_h$ of peptide aggregation into α -oligomer is somewhat lower (by the factor 0.78) than half of the average binding energy $b_h\epsilon_h = 155\epsilon_h$ that a fully folded peptide has in the bulk α -oligomeric phase. For comparison, in the Haas-Drenth lattice model[15] of protein crystals the latent heat of crystallisation is just half the average protein binding energy. Also, with $a = 4.0$ to 5.4 (see Fig. 3c), $\lambda = 15.1$ and $c = (36\pi)^{1/3}$, for the ratio $\sigma v^{2/3}/L = 3a/2c\lambda$ we obtain values from 0.08 to 0.11 in the θ range studied. Thus, $\sigma v^{2/3}/L$ for the α -oligomers is considerably smaller than for atomic or simple molecular substances which are known to follow the Stefan-Skapski-Turnbull relation $\sigma v^{2/3}/L = 0.2 - 0.6$ (e.g., Ref. [14]).

Next in our study was the determination of the γ -oligomer solubility. Following the procedure outlined for the α -oligomers, we prepared a cluster of size $n = 100$. As the γ -oligomer consists of fully folded, partially folded and unfolded peptides, their proportion in it was taken to be the same as that of the peptides in the solution at the

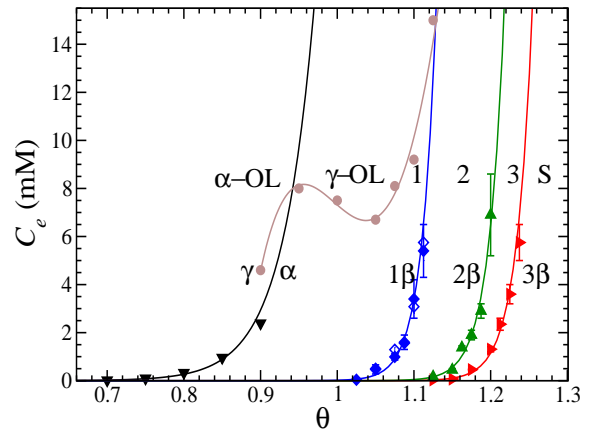


FIG. 4: Peptide phase diagram. Solubility-vs-temperature data for α -oligomer (down triangles) of infinitely large size, γ -oligomer (circles) of size $n = 100$, 1β -sheet (solid diamonds), 2β -sheet (up triangles) and 3β -sheet (right triangles), all of size $n = 40$. Lines α , 1β , 2β and 3β are obtained by best fit of equation 2 to the data; line γ is just a guide to the eye; labels α -OL, γ -OL, 1, 2, 3, and S refer to different stability regions (see main text); the open diamonds refer to $n = 20$.

chosen temperature. The simulations, in which we performed pivot, crankshaft, reptation, rotation and translation moves, revealed that the γ -oligomer was a transient formation always transforming into an $i\beta$ -sheet. For that reason it was necessary to use a biasing potential that arrested the γ -oligomer transformation by not allowing a peptide to form more than one interpeptide hydrogen bond with any other peptide in the cluster. The simulation $C_{e,n}(\theta)$ data for γ -oligomers of size $n = 100$ (the circles in Fig. 4) show that the γ -oligomer solubility cannot be described by equation 2. The non-monotonic behavior of the γ -oligomer solubility is a result of the temperature dependence of the proportion of folded and unfolded peptides in the oligomer. This effect is strongest for θ between 0.9 and 1.1, the temperature range in which the peptides commence unfolding and forming additional interpeptide hydrogen bonds that decrease the γ -oligomer solubility. Partial unfolding of proteins is regarded as being a crucial step in protein aggregation[17, 18] and our observation of the decreased γ -oligomer solubility with the peptide unfolding rationalizes this view. Regrettably, as the simulations with γ -oligomers were computationally much more demanding than those with the α -oligomers, we could not investigate the effect of the cluster size on the γ -oligomer solubility.

Finally, we determined the solubility lines for the 1β -, 2β - and 3β -sheets. In these simulations all $i\beta$ -sheets consisted of $n = 40$ unfolded peptides. Since $i\beta$ -sheet formation at a fixed i value is a one-dimensional clustering process, the $i\beta$ -sheet solubility is expected to be n -independent. We could not confirm this expectation for all $i = 1, 2$ and 3 , but simulations with 1β -sheets of size $n = 20$ revealed that these sheets indeed had the solubility of those with $n = 40$ (see the diamonds in

Fig. 4). The simulations showed also that a new peptide monolayer could occasionally form on the $i\beta$ -sheet studied, transforming it into an $(i + 1)\beta$ -sheet. In order to calculate the solubility of these metastable $i\beta$ -sheets we had to include a biasing potential preventing this transformation from occurring. The so-obtained simulation $C_{e,n}(\theta)$ data are shown in Fig. 4 by symbols. A fit of equation 2 to these data provides values for the reference peptide concentration and latent heat of peptide aggregation into an $i\beta$ -sheet: $C_r = 2.1 \times 10^{24}$ mM and $\lambda = 60 \pm 6$ for the 1β -sheet, $C_r = 4.3 \times 10^{24}$ mM and $\lambda = 66 \pm 4$ for the 2β -sheet, and $C_r = 1.2 \times 10^{24}$ mM and $\lambda = 66 \pm 3$ for the 3β -sheet. With the T_f value given above, it thus follows that $L = \lambda k T_f$ has the values of 12ϵ , 13.2ϵ and 13.2ϵ for the 1β -, 2β - and 3β -sheet, respectively. Again, these L values can be compared with the average binding energy $b\epsilon + b_h\epsilon_h = 22\epsilon$, 24ϵ and 24ϵ that an unfolded peptide has in the bulk 1β -, 2β - and 3β -sheet, respectively. These numbers follow from the b , b_h and ϵ/ϵ_h values already given above. We see that, similar to the α -oligomer, and in close correspondence with lattice models, for the $i\beta$ -sheets L is about half the peptide average binding energy. We note that the L value for the 3β -sheet may be regarded as representative for that of the infinitely thick β -sheet, because in our simulation model the hydrophobicity-mediated interaction is limited within two successive peptide monolayers only. This limitation is reflected by the virtually equal average binding energies of a peptide in the 2β - and 3β -sheets. Also, the L values for the $i\beta$ -sheets are considerably greater than those for the α - and γ -oligomers because of the presence of more hydrogen bonds per peptide in the $i\beta$ -sheets.

In conclusion, the phase diagram in Fig. 4 shows that there are two regions of thermodynamic stability, one of the peptide solution (region S), and one of the infinitely thick β -sheet. The dividing line between these two stable phases is approximately the solubility line of the 3β -sheet (line 3 β), because in our model the peptide interactions are restricted within two successive β -sheets. In addition to this, the phase diagram reveals the hierarchic existence of various metastable peptide phases. In region 3 the 3β -sheet is stable with respect to the solution, but metastable with respect to thicker $i\beta$ -sheets ($i > 3$). In region 2 the 2β -sheet is stable with respect to the solution, but metastable with respect to all thicker $i\beta$ -sheets ($i > 2$). In region 1 the 1β -sheet is stable with respect to the solution, but metastable with respect to all other $i\beta$ -sheets ($i > 1$). In region γ -OL the γ -oligomer is also stable with respect to the solution, but metastable with

respect to all $i\beta$ -sheets. Finally, in region α -OL, though being stable with respect to the solution, the α -oligomer is metastable with respect to all other aggregates. A similar hierarchy in the stability of protein aggregates has been observed in an experimentally obtained phase diagram of Human β B1-crystallin[3]. The high stability of the $i\beta$ -sheets arises from the fact that their structure is largely due to the preponderant presence of hydrogen bonds between the peptides[19]. Our finding of the existence of various metastable peptide phases and of hierarchy in their metastability provides a solid basis for describing the formation of amyloid fibrils and for understanding why these fibrils can grow out of disordered peptide aggregates[11, 20].

One of the authors (D. K.) gratefully acknowledges the financial support by the Leverhulme Trust (Grant F10100A) and the hospitality that he enjoyed as Leverhulme Visiting Professor at the University of Leeds.

-
- [1] N. Asherie, *Methods* **34**, 266 (2004).
 - [2] P. G. Vekilov, *Cryst. Growth Design* **4**, 671 (2004).
 - [3] O. Annunziata *et al.*, *Biochemistry* **44**, 1316 (2005).
 - [4] A. C. Dumetz, A. M. Chockla, E. W. Kaler, and A. M. Lenhoff, *Biophys. J.* **94**, 570 (2008).
 - [5] F. Chiti and C. M. Dobson, *Annu. Rev. Biochem.* **75**, 333 (2006).
 - [6] M. R. Sawaya *et al.*, *Nature* **447**, 453 (2007).
 - [7] R. I. Dima and D. Thirumalai, *Prot. Sci.* **11**, 1036 (2002).
 - [8] H. D. Nguyen and C. K. Hall, *Biophys. J.* **87**, 4122 (2004).
 - [9] T. X. Hoang, A. Trovato, F. Seno, J. R. Banavar, and A. Maritan, *Proc. Natl. Acad. Sci. USA* **101**, 7960 (2004).
 - [10] S. Auer, C. M. Dobson, and M. Vendruscolo, *HFSP J.* **1**, 137 (2007).
 - [11] S. Auer, C. M. Dobson, M. Vendruscolo, and A. Maritan, *Phys. Rev. Lett.* **101**, 258101 (2008).
 - [12] A. Saiani *et al.*, *Soft Matter* **5**, 193 (2009).
 - [13] X. M. Bai and M. Li, *J. Chem. Phys.* **124**, 124707 (2006).
 - [14] D. Kashchiev, *Nucleation: Basic Theory with Applications* (Butterworth-Heinemann, Oxford, 2000).
 - [15] C. Haas and J. Drenth, *J. Crystal Growth* **154**, 126 (1995).
 - [16] A. A. Chernov, *J. Struct. Biol.* **142**, 3 (2003).
 - [17] V. N. Uversky and A. L. Fink, *Biochim. Biophys. Acta* **1698**, 131 (2004).
 - [18] G. W. Platt *et al.*, *J. Mol. Biol.* **346**, 279 (2005).
 - [19] T. Knowles *et al.*, *Science* **318**, 1900 (2007).
 - [20] T. R. Serio *et al.*, *Science* **289**, 1317 (2000).